5462 J. Med. Chem. 2009, 52, 5462–5473
DOI: 10.1021/jm900599v

Journal of Medicinal Chemistry Article

Identification of Specific Small Molecule Ligands for Stem Loop 3 Ribonucleic Acid of the Packaging Signal Ψ of Human Immunodeficiency Virus-1

Douglas M. Warui and Anne M. Baranger*

Department of Chemistry, 361 Roger Adams Laboratory, University of Illinois, 600 South Mathews Avenue, Urbana, Illinois 61801

Received December 21, 2008

We have screened the NCI diversity set library for molecules that bind specifically to stem loop 3 (SL3) RNA of the packaging element Ψ of HIV-1 using the docking programs DOCK and AutoDock, followed by MD simulations. The association of the predicted ligands with SL3 RNA was characterized using fluorescence, ITC, UV-melting, CD, and footprinting techniques. Nine ligands for SL3 RNA have been identified, four of which bind with higher affinity to SL3 RNA than to either single- or double-stranded RNA motifs. The most selective ligands, **9** (NSC252359) and **5** (NSC123111), bind SL3 RNA with dissociation constants of 11 μM and 98 μM, respectively. Compound **9** binds with 4−7-fold higher affinity to SL3 RNA than to the other tetraloops found in Ψ-RNA, SL2 and SL4 RNAs. The results suggest that both **9** and **5** bind to the stem region of SL3 RNA without large distortions of the SL3 RNA.

Introduction

RNA plays essential functional roles in many steps of gene expression and regulation, including the regulation of transcription, translation, and RNA modification, including splicing.[1,2] Thus, molecules able to bind specifically to particular RNA sequences and structures and alter RNA function could be powerful tools for understanding and controlling gene expression.[3−5] RNA folds to form complex secondary and tertiary structures that are important for RNA function. One of the most basic classes of secondary structure is the RNA hairpin. Although RNA hairpins play vital roles in biological processes involving RNA, form target sites for both proteins and other RNAs, and are the most abundant form of secondary structure after the helix,[6−15] there has been little investigation of small molecule binding to RNA hairpins.[3] We previously developed a computational docking method to identify ligands that bind to GNRA tetraloops.[16] We report here the application of this approach to discover specific small molecule ligands for an RNA stem loop (SL3) that is essential for packaging of HIV.

The major packaging domain of HIV-1 retrovirus, called the packaging element Ψ or Ψ-site, is comprised of four stem loops, SL1−4 (Figure 1).[17,18] Although all four stem loops play important roles in the replication process of the virus, SL3[a] plays a critical role as part of the principle recognition and packaging determinant for efficient encapsulation of the viral genome.[17,19−27] SL3 is a GGAG hairpin and is highly conserved among different strains of HIV-1.[18,28] Previous NMR studies of the structure of SL3 RNA suggest that the loop forms a dynamic structure that may be more adaptable to binding small molecule ligands than the GNRA tetraloops we investigated previously.[23] This hypothesis is supported by the binding of aminoglycosides and some other well-characterized RNA ligands to the Ψ-site and the individual stem loops in the Ψ-site with micromolar affinity, while most of these ligands do not bind well to GNRA loops.[29−33] Phage display techniques have been used to select peptides that bind to the Ψ-site and to individual stem loops within the Ψ-site.[34] One of these selected peptides that binds SL3 RNA was shown to reduce virus release by infected cells.[35] Thus, although SL3 RNA is not a target of current anti-HIV therapeutics, the development of small molecules that bind SL3 RNA could lead to novel anti-HIV agents.

To identify new RNA binding scaffolds for SL3 RNA, we have screened a library of compounds using computational methods that include the programs DOCK and AutoDock supplemented with molecular dynamics (MD) simulations. DOCK uses shape complimentarity to match the ligand to the binding site of the receptor.[36−38] The accuracy of DOCK is limited by its simple scoring function, which exclusively considers van der Waals and electrostatic interactions. AutoDock uses a more exhaustive scoring function that includes desolvation, hydrogen bonding, ligand torsional, van der Waals, and electrostatic energies.[39] Although the development of computational methods to identify small molecule ligands for nucleic acids is still at early stages of development, the ability of DOCK and AutoDock to accurately reproduce the structures and relative stabilities of nucleic acid−small molecule complexes has been validated in several independent investigations.[40−46] Previous docking investigations performed in our laboratory and other laboratories suggest that sequential docking with Dock followed by AutoDock is a better strategy than using either program alone for identifying small-molecule ligands for nucleic acids.[16,42,46]

We have screened the NCI diversity set for binding to the major groove proximal to the flexible loop of SL3 RNA and have identified nine molecules that bind SL3 RNA with micromolar affinity. We have characterized the binding affinity

*To whom correspondence should be addressed. Phone: (217) 244-7649. Fax: (217) 244-8024. E-mail: baranger@uiuc.edu; Baranger@illinois.edu. University of Illinois at Urbana−Champaign, Department of Chemistry, 361 Roger Adams Laboratory, Box 41-5 600, South Mathews Avenue, Urbana, IL 61801.

[a] Abbreviations: SL3, stem loop 3; MD, molecular dynamics; MOE, molecular operating environment.

 Published on Web 08/19/2009

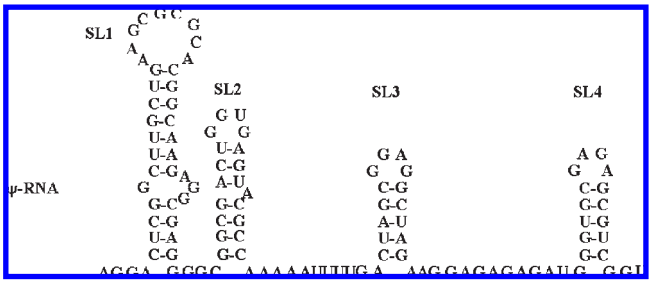

Figure 1. Sequence of the HIV-1 genomic RNA packaging signal Ψ.[25]

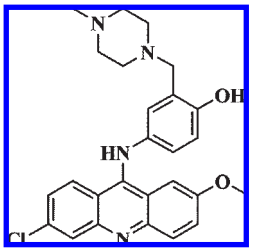

Figure 2. Structure of AD2.

of these molecules and the specificity of a subset of these molecules for SL3 RNA over SL2 and SL4 RNAs and double- and single-stranded RNA sequences. These investigations have revealed two molecules, **9** (NSC252359) and **5** (NSC123111), that bind with higher affinity to SL3 than to double- and single-stranded RNAs. Compound **9** binds with 4-fold and 7-fold higher affinity to SL3 RNA than to SL2 and SL4 RNA, respectively. Thus, the computational screening method has identified a molecule that binds selectively to SL3 RNA with micromolar affinity.

Results and Discussion

Investigation of the Binding of AD2 to SL3 RNA. We previously used computational docking to identify an acridine derivative, AD2 (Figure 2), that binds to a GNRA tetraloop hairpin RNA with a K_D of 1 μM.[16] AD2 is specific for the GNRA tetraloop over both single- and double-stranded RNA. Because SL3 is also a tetraloop, we initiated our investigation of small molecule ligands of SL3 RNA by determining the ability of AD2 to bind specifically to SL3 RNA. AD2 binds to SL3 with high affinity ($K_D = 0.67$ μM, Table 1). However, AD2 binds equally well to double-stranded RNA under the conditions used in these experiments and only 4.4-fold weaker to single-stranded RNA (Table 2). Although AD2 binds tightly to SL3 RNA, it does not do so specifically. Therefore, a goal of the computational docking described here was to identify molecules able to bind specifically to SL3 RNA.

Selection of Binding Site and Overall Docking Strategy. Structures of both the free SL3 RNA and the complex formed with the NC protein have been determined by NMR spectroscopy.[18,23] The structure of the free SL3 RNA revealed a highly flexible loop that is constrained upon interaction with the NC protein. Because the free and bound SL3 RNA structures are similar except for the loop region, the structure of the bound SL3 RNA was used as the target for computational docking. The docking site was defined as the major groove region proximal to the flexible loop area

Table 1. Summary of Experimentally Determined Dissociation Constants by Fluorescence Methods for the Compounds Identified through Computational Docking Studies

compd	mol wt (g mol^{-1})	formal charge[d]	K_D (μM)[f]
AD2[a]	463	2	0.67 ± 0.03
3[a]	319	0	1.4 ± 0.4
6[a]	249	2	1.5 ± 0.7
9[b]	342	0	11 ± 3
2[a,c]	352	0	32 ± 1
5[b]	331	0[e]	98 ± 43
4[b,c]	320	0	118 ± 63
8 (NSC121848)[a]	316	1	135 ± 48
1 (NSC61809)[b]	318	1	157 ± 18
7 (NSC657704)[a]	376	0	163 ± 2

[a] Dissociation constants determined by titration of ligands to fluorescein-labeled 20mer SL3 RNA. [b] Dissociation constants determined by titration of ligands to fluorescein-labeled 14mer SL3 RNA. [c] The K_Ds of **4** and **2** were determined by reverse titration with unlabeled 14mer SL3. [d] Formal charges as determined by MOE. [e] Compound **5** was assigned a formal charge of zero by MOE, but a formal charge of 1 was predicted using Advanced Chemistry Development (ACD/Laboratories) Software V8.14 for Solaris. Compound **5** was uncharged in the computational docking. [f] Errors are the standard deviation of at least three independent measurements.

(Figure 3). This site is similar to the docking site we used previously to find ligands for GNRA tetraloop targets and is the site of interaction of a 3_{10} helix of the NC protein.[16,18]

Computational docking was performed with the National Cancer Institute (NCI) diversity set database, which is comprised of 1990 compounds that have been selected from 140000 compounds based on pharmacophore diversity and a minimum available quantity at the NCI. We selected this set of molecules to screen because it is a relatively small library of drug-like molecules. Selected compounds are easily obtained from the NCI, which is important because docking of small molecules to RNA is not well-developed and therefore, may lead to false hits. We used Molecular Operating Environment (MOE) software (Chemical Computing Group) to retain compounds with molecular weights less than or equal to 500, log P values less than or equal to 4, 10 or fewer total number of rotatable bonds, and a neutral or positive formal charge. This screening eliminated 31% of the library, resulting in 1367 compounds, ~5% of which carried at least one positive charge.

Computational Screening of Compound Library. A stepwise computational screening process began by using the program DOCK to identify SL3 RNA ligands within the selected 1367 compounds. DOCK uses shape complimentarity to match the ligand to the binding site of the receptor by generating a sphere file to represent the docking site.[36−38] The docking site was chosen and manually assigned 100 spheres. The number of spheres used was within the range recommended by the developers of DOCK.[47] The potential binding site for the ligands was chosen to include the junction region between the loop and the major groove of SL3 RNA in order to identify ligands that would exhibit selectivity against nonhairpin structures. The selected spheres were then used to define the scoring grid and docking site. The edges of the scoring grid that defined the docking site are shown in Figure 3. The library compounds were assigned partial atomic charges using the Gasteiger (PEOE) force field in the MOE program. The compounds were ranked by their energy scores determined by DOCK, and the top 8% were retained for further screening with the program AutoDock. AutoDock[39] allows for the efficient semirigid docking of a

Table 2. Summary of Experimentally Determined Dissociation Constants Using Fluorescence Methods for AD2 and the Four Compounds that Demonstrated Selectivity for SL3 RNA over Both Single- and Double-Stranded RNA Sequences[a]

compd	SL3 RNA	duplex RNA K_D (μM)	single-stranded RNA K_D (μM)	SL3 duplex RNA K_D (μM)
AD2	0.67 ± 0.03	0.87 ± 0.05	3.0 ± 0.3	ND
3	1.4 ± 0.4	3 ± 1	2.3 ± 0.1	NS
6	1.5 ± 0.7	6.1 ± 0.9	7.8 ± 0.3	14 ± 5
9	11 ± 3	69 ± 12	276 ± 50	58 (±1)
5	98 ± 43	345 ± 39	> 4900	NS[b]

[a] Errors are the standard deviation of at least three independent measurements. [b] ND is not determined and NS is no significant fluorescence signal change was observed upon addition of ligand to the SL3 duplex RNA labeled with fluorescein at the 5′ end.

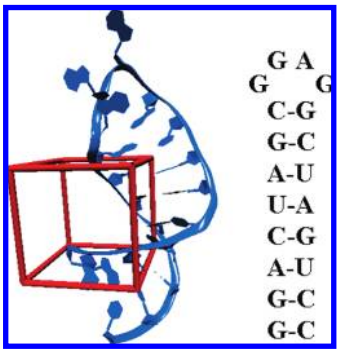

Figure 3. Structure of SL3 hairpin (blue, PDB ID 1A1T), the edges of the energy scoring grid for the computational docking (red), and the sequence of SL3 RNA.

flexible ligand to a rigid target molecule. AutoDock predicted binding energy scores of ≤ −11 kcal/mol for 30 compounds, which are shown in Figure 4. The selected structures share common features of aromatic and heteroaromatic groups that could stack with the RNA bases and a variety of other functional groups that may participate in hydrogen bonding with hydrogen bond donors and acceptors on the RNA. Seven of 30 (23%) of the selected molecules contain positively charged groups, compared to ∼5% in the initial pool of molecules. It is not surprising that the fraction of molecules containing positive charges has increased in the selection process because the positively charged groups should interact favorably with the phosphate backbone of RNA.

MD Simulations of Representative SL3-Ligand Complexes. Of the 30 compounds identified by AutoDock, the 10 best-ranked compounds were selected for MD simulation studies to predict the flexibility and stability of their complexes with RNA in solution. The docking process using both DOCK and AutoDock programs only includes conformational flexibility of the ligands, not the RNA receptor. Although the docking site selected on SL3 RNA is structurally stable by NMR, the adjacent loop is dynamic, and these dynamic processes could alter the binding site of the ligand. Therefore, we performed MD simulations to probe whether the structure of the ligand−RNA complex predicted by AutoDock would be different if SL3 RNA were allowed conformational flexibility.

To identify possible binding modes of representative compounds and to give a qualitative picture of conformational dynamics of their complexes with SL3 RNA, we performed 5 ns MD simulations using an all-atom force field with explicit water and counterions.[48,49] Although exhaustive sampling of the dynamics of the ligand−SL3 RNA complexes cannot be expected within 5 ns, a qualitative description of their conformational flexibility should result from these simulations. With this goal in mind, the structures predicted by AutoDock to be most stable were used as initial structures for the MD simulations. The initial structures and snapshots from the last 0.5 ns of the 5 ns simulations are shown for each of the ligand−SL3 RNA complexes in Figure 5a. Two of the 10 ligands (**22** (NSC357756) and **25** (NSC303530)) dissociated from the RNA during the course of the simulations. Two ligands (**3** (NSC119236) and **14** (NSC633406)) remained bound to the RNA but to different binding sites than those predicted by AutoDock. The remaining six complexes were stable, and the ligands remained bound within the binding site predicted by AutoDock, although in different binding poses.

The results of the MD simulations can be compared to the experimental results described in more detail in the next section. Of the 10 compounds described here, seven were studied experimentally, one was not soluble and could not be studied experimentally, and two could not be identified and were assumed to be degraded or impure. Thus, the binding of six of the eight molecules that remained bound to the RNA during the MD simulations was characterized experimentally. Binding to SL3 RNA was observed for five of the six molecules. The sixth molecule, compound **29** (NSC119847), was assumed not to bind SL3 RNA because no fluorescence change was observed upon its addition to 5′-fluorescein-labeled SL3 RNA. However, it is possible that **29** does bind to SL3, but this binding does not alter the fluorescence signal. The limited solubility of **29** precluded measuring binding by ITC. The binding of one of the two compounds that dissociated from the RNA during the MD simulations was studied experimentally, compound **25**, while the other molecule, compound **22**, was not studied experimentally because of its poor solubility in water and DMSO. Consistent with the MD simulations, fluorescence binding experiments suggest that **25** does not bind to SL3 RNA.

Analysis of the MD simulations showed that the loop bases of the SL3 hairpin were flexible and adopted various conformations in the course of the simulations in general, while the stem helix bases remained fairly stable with minimal conformational perturbations, which is consistent with structural investigations of the SL3 RNA by NMR spectroscopy.[23] Rmsd analyses of the backbone atoms of the RNA in the MD simulations of the free RNA and the RNA complexed with the most selective ligands, **5** and **9**, are presented in Figure 5b. Interestingly, the complex formed with **9** shows the greatest fluctuations in structure, especially during the first 2 ns. All three simulations have equilibrated by 2.5−3 ns to structures 2−3 Å away from the original structure predicted by AutoDock. The equilibrated structures are dynamic, and the binding of the ligands does not reduce the dynamics indicated in these analyses.

An analysis of the average structures of **5** and **9** in complex with SL3 RNA extracted from the simulations suggested that, in addition to van der Waals interactions, intermolecular

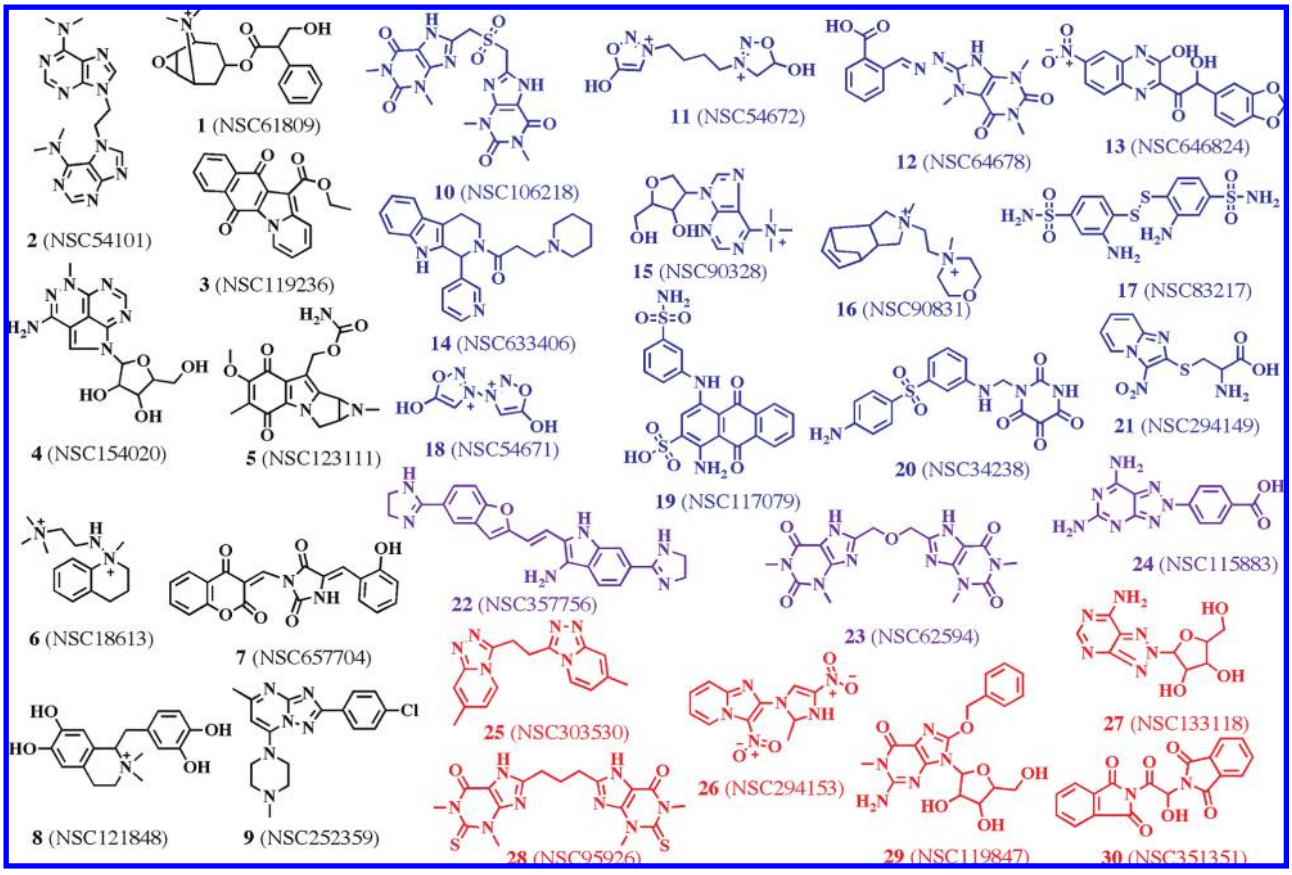

Figure 4. Compounds from virtual screening for which AutoDock predicted binding energy scores of ≤ −11 kcal/mol. The charges assigned to the molecules for computational docking are indicated in the drawing. Highlighted in black are compounds whose identities were confirmed and which bound SL3 RNA, in red are compounds whose identities were confirmed, but which did not bind SL3 RNA, in blue are compounds whose identities could not be confirmed, and in purple are compounds that were not soluble under the binding conditions.

hydrogen bonds are important for binding between SL3 and the ligands. Compound **5** forms four hydrogen bonds with the RNA, two with the 4-NH_2 group of C14, and one each with O6 of G9 and the phosphate group of G12, while **9** is stabilized by a single hydrogen bond formed between a piperazine amino group and O6 of G17. In addition, the complex with **5** appears to be stabilized by charge−charge electrostatic interactions between the amino group of the aziridine ring and the phosphate group of G12.

Experimental Screening of Selected Compounds. The 30 compounds predicted by AutoDock to form complexes with SL3 RNA with a binding energy of ≤ −11 kcal/mol were obtained from the NCI and screened experimentally. Three of the selected compounds (**22**, **23** (NSC62594), and **24** (NSC115883)) were insoluble in water and DMSO and therefore were not considered further. The identities of the remaining 27 compounds were evaluated by ESI mass spectrometry. The ESI spectra of 15 of the 27 compounds contained the correct molecular ion peak. The identities of three of the remaining 12 compounds (**19** (NSC117079), **20** (NSC34238), and **10** (NSC106218)) were further evaluated using FAB, EI, and CI mass spectrometry and NMR spectroscopy, and the spectra obtained were not consistent with the expected structures. Therefore, only the 15 correctly identified compounds were screened for binding to SL3 RNA.

The binding affinities of the selected molecules to a 20mer SL3 RNA were measured by fluorescence spectroscopy. A fluorescein label was introduced into the 5′-terminus of SL3 RNA and changes in the fluorescence signal (either quenching or enhancement) were monitored as a function of ligand concentration. This general method for determining binding affinity, in which a change in the conformation of the RNA stem loop upon ligand binding results in a change in the fluorescence signal of fluorescein, has been used extensively to determine the binding constants of RNA−ligand complexes.[3,50−52] Although some binding events may not be detected by this method, those K_D's that are measured are similar to those measured using other methods. For each binding experiment, a control experiment was performed in which the ligand was titrated into a solution of free fluorescein to probe for the possibility of a direct interaction between the ligand and fluorescein. None of the small molecules studied altered the fluorescence of fluorescein in the control experiments. The addition of two of the molecules, **2** (NSC54101) and **4** (NSC154020), to the fluorescein-labeled SL3 RNA did not result in a significant change in fluorescence. Because both compounds were intrinsically fluorescent, their affinities for SL3 RNA were determined by reverse titration with unlabeled 14mer SL3 RNA.

Nine of the 15 selected molecules were found to bind SL3 RNA using the methods described above. Apparent dissociation constants were obtained assuming a 1:1 stoichiometry of ligand to SL3 RNA and are listed in Table 1. Of the six compounds found not to bind SL3 RNA, three were sparingly soluble under the experimental conditions and therefore binding at higher ligand concentrations may have been prevented by low ligand solubility. It is also possible that

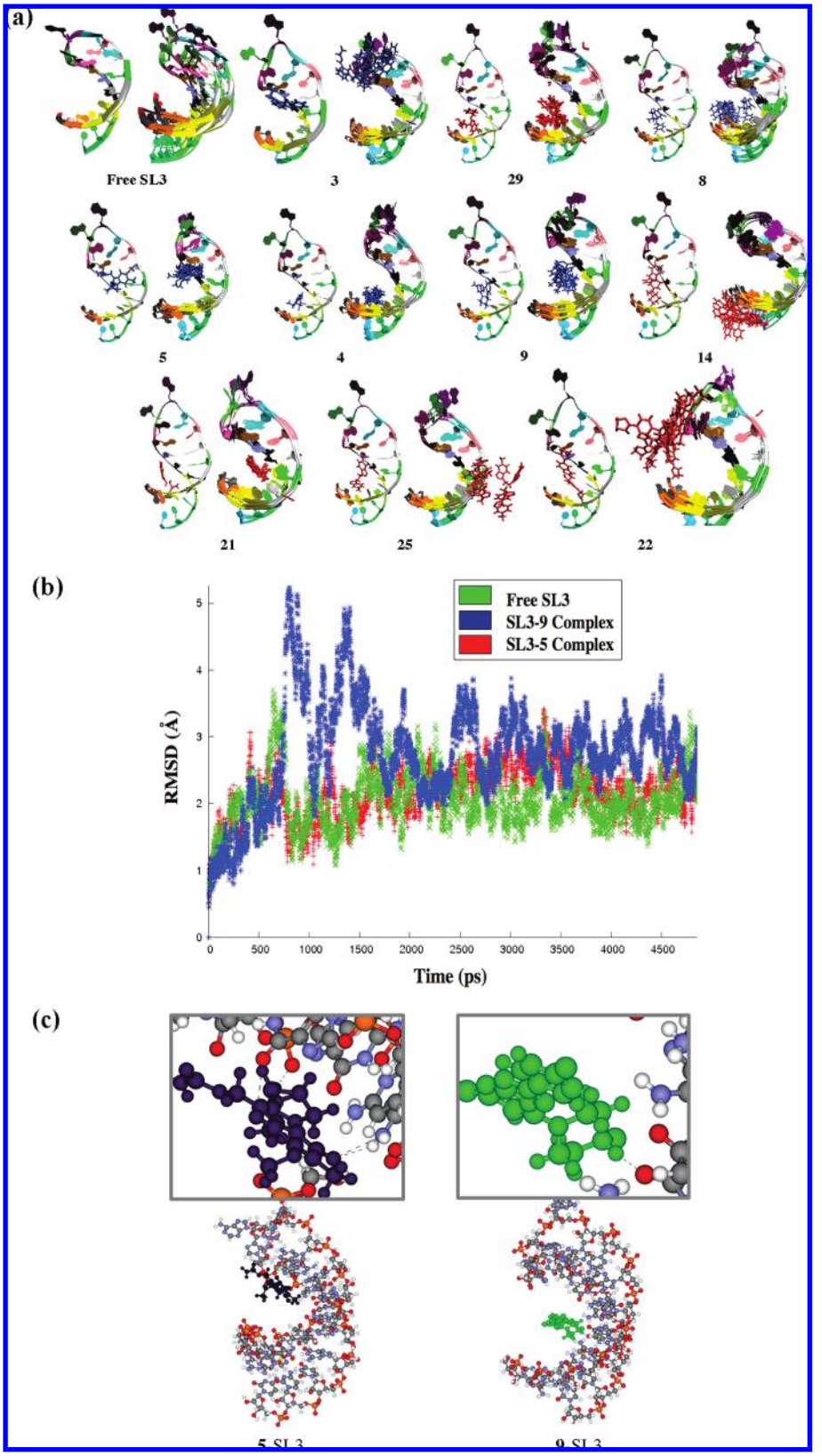

Figure 5. (a) MD simulation snapshots of the 10 SL3 RNA−ligand complexes taken at 0 ns and the last 0.5 ns (overlaid structures with 100 ps intervals) of the 5 ns simulation. (b) Plots of the rmsd of the RNA backbone atoms from the equilibrated structures calculated over the course of the MD trajectories. In green is free SL3 RNA, blue is SL3 RNA in complex with **9**, and red is SL3 RNA in complex with **5**. (c) Average MD structures of **5** (left, purple) and **9** (right, green) in complex with SL3 RNA. Intermolecular H-bonding interactions formed between the ligands and SL3 RNA are indicated with gray dashed lines in the inset.

these compounds did bind to the RNA but did not alter the fluorescence of fluorescein-labeled SL3 RNA upon binding. The six compounds were not fluorescent, and hence binding could not be determined by reverse titration methods.

Because of the high sample concentrations required to measure binding by ITC, especially for low-affinity binders, we could not use ITC to confirm that these six molecules do not bind SL3 RNA. Thus, these six molecules were not investigated further.

Specificity of Selected Ligands for SL3 RNA. The selectivity of four of the molecules that bind SL3 RNA with highest affinity (**3**, **5**, **6** (NSC18613), and **9**) compared to double- and single-stranded RNA sequences was investigated. These four molecules contain functionalities typical of RNA binding molecules. Compound **3** is a large flat aromatic molecule that would be expected to intercalate at the junction between the stem and the loop. Compound **6** is quite small, and therefore it is surprising that it binds relatively strongly to the RNA, although the three positive charges are expected to contribute favorably to binding. Compound **9** contains aromatic groups to stack with RNA bases, although the MD simulations and CD experiments suggest that stacking interactions are not formed in the complex and heteroatoms participate in hydrogen bonds. Finally, **5** is a derivative of mitomycin C, which covalently modifies the 2-amino group of guanine in CG sequences in DNA.[53,54] Although mitomycin C requires a reductant to react with DNA, this particular derivative is able to form covalent adducts with DNA in the absence of a reductant.[53,55] We investigated whether **5** is forming covalent adducts with RNA upon binding under the conditions used in this paper, which include lower concentrations of **5** than is typical for investigations of covalent modification. The SL3 RNA was incubated with **5** for 72 h at room temperature. Analysis of the sample using MALDI mass spectrometry did not show a peak with a higher mass consistent with the formation of a covalent adduct, suggesting that the RNA is not covalently modified upon binding of **5** under the binding conditions used in this investigation.

The double- and single-stranded RNA sequences used in these experiments are shown in Figure 6. All of the RNAs were labeled at the 5′-end, and binding was monitored by measuring quenching or enhancement of the fluorescence signal. Binding to two different double-stranded RNA sequences was investigated. One of the double-stranded sequences is identical to that used to determine the specificity of AD2 for GNRA tetraloops,[16] while the other is identical to the stem sequence of the 20mer SL3 sequence. The results of these experiments are presented in Table 2 and Figures 7 and 8. Compound **3** bound with 2-fold higher affinity to SL3 RNA than to double- and single-stranded sequences. No change in the fluorescence signal of the SL3 duplex RNA was observed upon addition of **3**. Compound **6** bound with 4- to 9-fold greater affinity to SL3 RNA than to single-stranded and both double-stranded RNA sequences. In contrast, although **9** and **5** bound with lower affinity to SL3 RNA than the other two molecules, they showed similar specificity for SL3 RNA over the double-stranded RNA sequences and greater specificity for SL3 RNA over the single-stranded sequences. Compound **9** bound with 5−6-fold lower affinity to both double-stranded RNA sequences and 25-fold lower

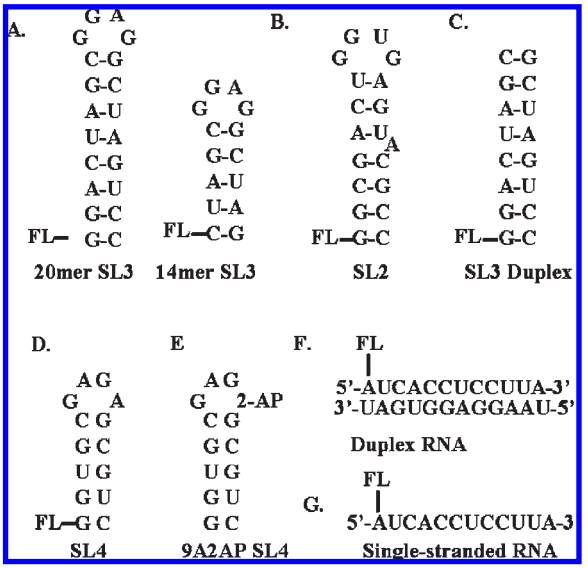

Figure 6. RNA sequences used in the fluorescence assays. Each of the sequences was labeled at the 5′ end with fluorescein, abbreviated FL, except 9A2AP SL4, which was labeled in the loop by substituting adenine at position 9 with the fluorescent 2-aminopurine nucleotide.

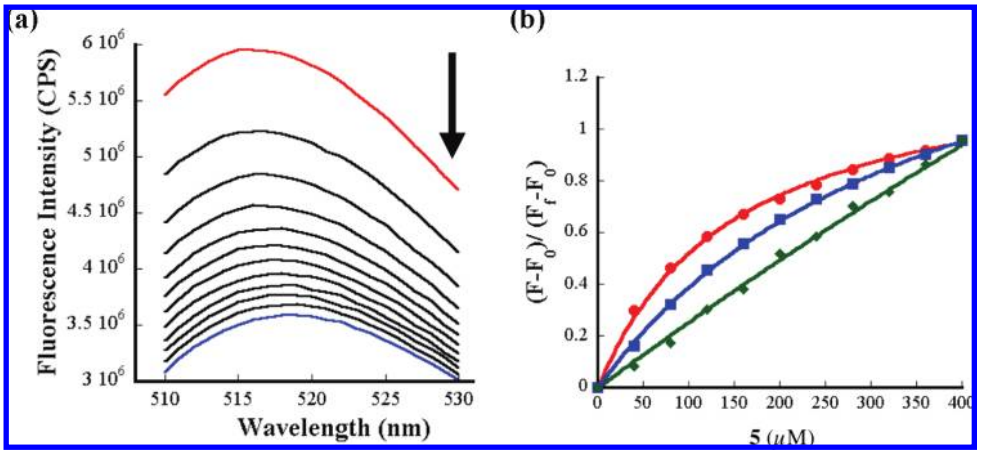

Figure 7. (a) Fluorescence quenching of 5′ fluorescein labeled 14mer SL3 RNA (25 nM) upon addition of **5**. Experiments were performed in 10 mM Tris·HCl (pH 7.4), 25 mM NaCl at 25 °C. The concentration of **5** was varied between 30 and 360 μM. The spectrum of free SL3 RNA is shown in red, while the saturation point (addition of 360 μM **5**) is shown in blue. Samples were excited at 490 nm, and emission was monitored from 510 to 530 nm. Emission at 517 nm was used to calculate the fraction of RNA bound by **5**. (b) Representative binding curves of the complexes formed between **5** and SL3 (red), double-stranded (blue), and single-stranded (green) RNAs. The data were fit with eq 1 assuming a 1:1 stoichiometry as described in the text.

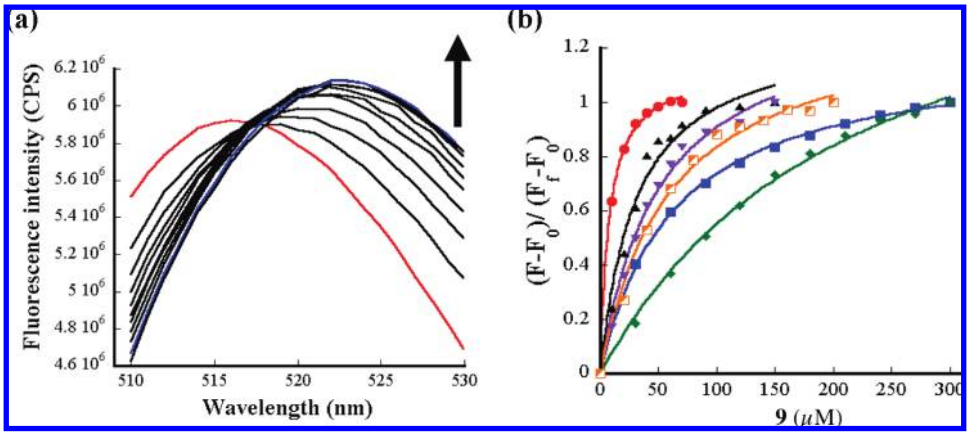

Figure 8. (a) Fluorescence enhancement of 5′-fluorescein labeled 14mer SL3 RNA (25 nM) upon addition of **9**. Experiments were performed in 10 mM Tris·HCl (pH 7.4), 25 mM NaCl at 25 °C. The concentration of **9** was varied between 10 and 100 μM. The spectrum of free SL3 RNA is shown in red, while the saturation point (addition of 100 μM **9**) is shown in blue. Samples were excited at 490 nm, and emission was monitored from 510 to 530 nm. Emission at 525 nm was used to calculate the fraction of RNA bound by **9**. (b) Representative binding curves of the complexes formed with **9** and SL3 (red), duplex SL3 (orange), double-stranded (blue), single-stranded (green), SL2 (black), and SL4 (purple) RNAs. The data were fit with eq 1 assuming a 1:1 stoichiometry as described in the text.

Table 3. Summary of Dissociation Constants Determined for Complexes Formed between **5** and the Indicated RNAs[a]

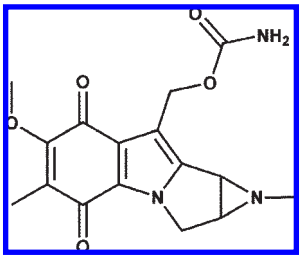

RNA motif	fluorescence K_D (μM)	ITC K_D (μM)
SL3	98 (±43)	110 (±27)
		11000 (±4000)
SL2	NS	ND
SL4	79 (±13)[b]	ND
duplex	345 (±39)	ND
single stranded	>4900	ND

[a] Errors are the standard deviation of at least three independent measurements. NS is no change in fluorescence signal was observed upon addition of **5** to labeled SL2 and ND is not determined. [b] Determined by addition of **5** to 2-aminopurine-labeled SL4 RNA.

Table 4. Summary of Dissociation Constants Determined for Complexes Formed between **9** and the Indicated RNAs[a]

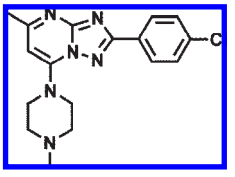

RNA motif	fluorescence K_D (μM)	ITC K_D (μM)
SL3	11 (±3)	15 (±3)
		2250 (±636)
SL2	46 (±9)	ND
SL4	70 (±4)	ND
SL3 duplex	58 (±1)	ND
duplex	69 (±12)	ND
single stranded	276 (±50)	ND

[a] Errors are the standard deviation of at least three independent measurements. ND is not determined.

affinity to single-stranded RNA, while **5** bound with 3.5-fold and 50-fold lower affinity to double-stranded and single-stranded RNA sequences, respectively. No change in the fluorescence signal of the SL3 duplex RNA was observed upon addition of **5**. However, **5** may bind to the SL3 duplex and not change the fluorescence signal of fluorescein. Because specificity of RNA-binding compounds for particular targets is more difficult to achieve than affinity, we focused the remaining investigations on the most specific SL3 binding compounds, **9** and **5**.

We investigated whether **9** and **5** are specific for SL3 RNA over the other two stem loops in Ψ RNA, SL2 and SL4, using fluorescence assays with the sequences shown in Figure 6. The data are presented in Tables 3 and 4. Similar to SL3 RNA, the stem loops were labeled on the 5′-end with fluorescein, and quenching or enhancement of the fluorescence signal was monitored as a function of added ligand.

Addition of **5** to 5′- fluorescein-labeled SL2 and SL4 RNAs resulted in an insignificant change of the fluorescence signal up to a concentration of 200 μM. Thus, to determine the K_D of **5** for SL4, the RNA was labeled at the loop by substituting adenine at position 9 with 2-aminopurine. The data showed that **5** binds to both SL3 and SL4 RNAs with similar affinities (Table 3). Although the binding affinity of **5** for SL3 was confirmed using ITC, a similar approach with SL2 and SL4 was not undertaken because of the high sample concentrations required. In contrast, addition of **9** led to significant fluorescence signal change of both 5′-fluorescein labeled SL2 and SL4 RNAs. The data showed that **9** binds with 4-fold and 6-fold greater affinity to SL3 RNA than to SL2 and SL4 RNAs, respectively (Table 4). Thus, **9** binds with higher affinity to SL3 RNA than to either SL2 or SL4 RNA.

Isothermal Titration Calorimetry (ITC) Assays. The binding of two of the most selective compounds, **9** and **5**, to SL3 RNA was further investigated using ITC. The data were fit using a two-site sequential binding model for both compounds (Figure 9). The dissociation constants obtained for **9**

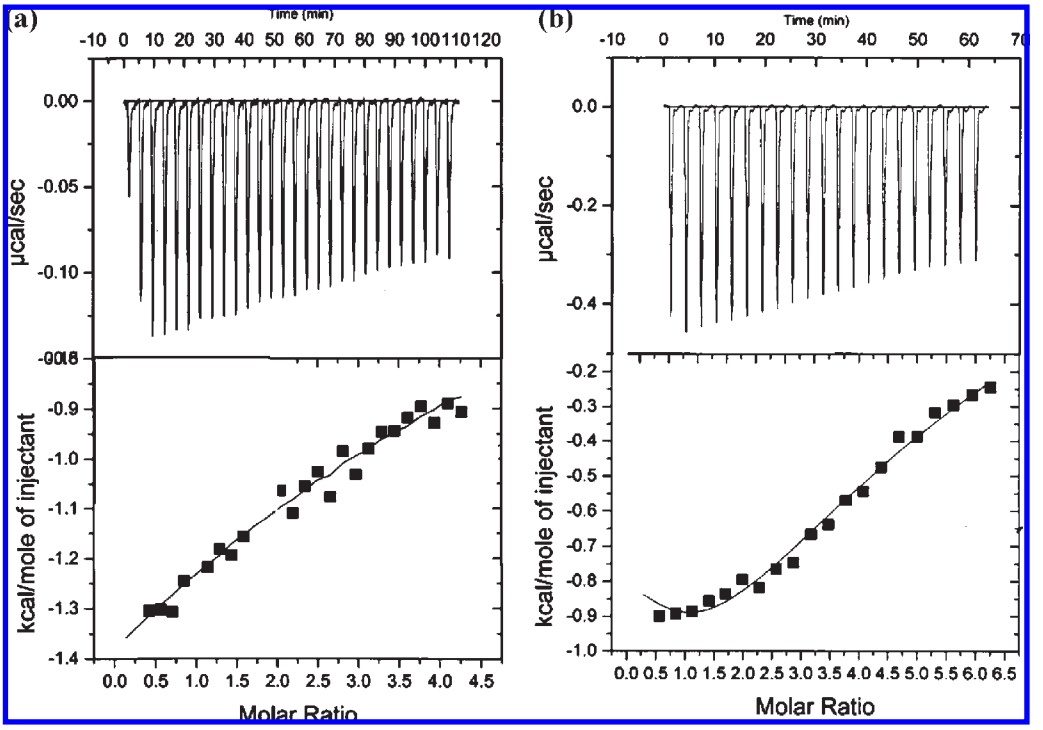

Figure 9. Representative ITC profiles for the titration of (a) **5** and (b) **9** into a solution of unlabeled SL3 RNA (20 μM) in 10 mM Tris·HCl (pH 7.4), 25 mM NaCl buffer at 25 °C. Each heat burst, shown in the upper curves, is the result of a 10 μL injection of 500 μM of compound (a) **5** and (b) **9**. The corrected injection heats shown in the bottom curves were derived by integration of the corresponding heat bursts (upper curves) followed by subtraction of the corresponding dilution heats derived from control titrations of each compound into buffer alone. The data points in the bottom curves reflect the corrected experimental injection heats, while the continuous lines reflect the calculated fits of the data using a sequential two site binding model.

were 15 ± 3 and 2.3 ± 0.6 mM, while the dissociation constants obtained for **5** were 110 ± 27 and 11 ± 4 mM. Thus, the ITC titrations suggested that the ligands are binding to a stronger and a weaker binding site. The dissociation constants for the tighter binding site from ITC are consistent with those obtained using the fluorescence methods described above (Tables 3 and 4), while the lower affinity binding site was not detected in the fluorescence assays.

Characterization of the Structure and Stability of SL3 RNA upon Binding Selected Ligands. The effects of ligand binding on the stability of SL3 RNA were investigated by UV melting experiments. Both the free and the bound SL3 RNA melting curves showed single sharp transitions indicating that the RNA predominantly existed as single species. Analysis of the UV melting data showed that SL3 RNA is stable thermally with a T_m of 77.3 (±1.1) °C (25 mM NaCl). SL3 RNA showed a slight stabilization of ~1−2 °C upon binding of compounds **9** (78.2 ± 1.1 °C) and **5** (79.2 ± 0.7 °C). These small changes in the RNA melting temperature are within experimental error, which suggests that the binding of either ligand does not dramatically affect SL3 RNA thermal stability.

To probe whether binding of the selected compounds **5** and **9** changed the conformation of SL3 RNA, the structure of SL3 was investigated using CD spectroscopy (Figure 10). The CD spectrum showed a negative signal at 238 nm and a positive signal at 260 nm, indicating the presence of an A-form helix, and a shoulder at 280 nm, indicating the presence of a loop structure,[56−59] thus confirming formation of an RNA hairpin. Addition of **5** to SL3 RNA led to a significant gradual decrease of the signal at 238 nm along with smaller changes to the 260 and 280 nm signals. This observation rules out a binding mode involving pure intercalation, which would have resulted in a dramatic CD spectral change at 260 nm, and suggests that **5** interacts with the helical stem region of the RNA and perturbs the loop region (Figure 10a). Unlike **5**, addition of **9** to SL3 RNA did not alter the RNA CD spectrum (Figure 10b). This observation ruled out binding through intercalation or to the flexible loop region, suggesting that **9** interacts with the RNA stem without altering the RNA structure. Overall the UV and CD results suggest that the RNA conformation and stability is not dramatically altered upon addition of either **5** or **9** at the concentrations required for binding, which is consistent with the results of the MD simulations.

Characterization of the Binding Site of 5 and 9 by Footprinting Experiments. To characterize the binding site of **5** and **9** on SL3 RNA, footprinting studies were performed. We selected RNase I and lead acetate cleavage reagents for footprinting because they have been shown to cleave RNA tetraloops.[33] Both reagents cleave single-stranded RNA with no base specificity and double-stranded regions that contain weak, bulged, or destabilized base pairs.[60,61] However, RNase I footprinting experiments were not reproducible and were difficult to analyze. Therefore, results from lead acetate footprinting experiments, shown in Figure 11, are described here. Analysis of the lead acetate footprinting cleavage results for **5** showed increased protection of all bases in general, with the exception of C5, which is part of the base pair that closes the loop. Further analysis showed that the first four bases of the RNA had the highest protection relative to the remainder of the RNA sequence, which is consistent with binding to the stem region as also predicted by both AutoDock and MD simulations, although both

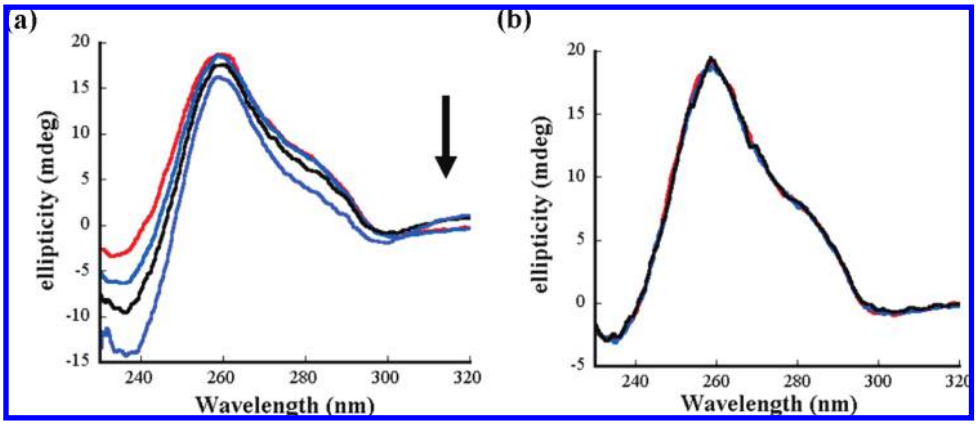

Figure 10. CD spectra showing the signal change of SL3 RNA with addition of **5** and **9**. Experiments were performed with 15 μM SL3 RNA in 10 mM Tris·HCl pH 7.4, 25 mM NaCl buffer at room temperature. (a) Spectral change of SL3 RNA (red) upon addition of 55 μM (blue), 110 μM (black), and 220 μM (purple) of **5**. (b) No significant spectral change of SL3 RNA (red) was observed upon addition of 55 μM (blue) and 110 μM of **9** (black).

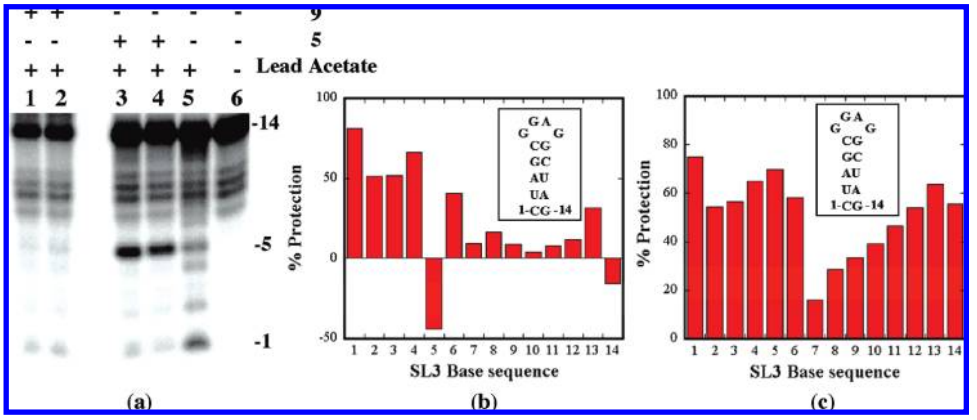

Figure 11. (a) Footprinting autoradiogram of SL3 RNA using lead acetate in the presence of the ligands **9** and **5**. Lanes 1 and 2, 500 μM **9**, lanes 3 and 4, 500 μM **5**, and lane 5 is the RNA only control. (b) Plots of lead acetate cleavage results of SL3 RNA in complex with **5** and (c) SL3 RNA in complex with **9**. Inset is the SL3 RNA sequence used in the foot printing experiments. Positive numbers indicate increased protection and negative numbers indicate decreased protection of individual nucleotide bases of the RNA sequence in the presence of the ligands relative to protection of the bases in absence of the ligands.

AutoDock and the MD simulations predicted interactions between the base of the loop and **5**. Analysis of lead acetate cleavage results of the complex formed between SL3 RNA and **9** showed an overall increased protection of all the nucleotides. The stem bases had the highest protection and the loop bases had decreased relative protection. This suggests that **9** also binds to the stem region of SL3 RNA, consistent with the computationally predicted binding site.

Conclusion

We have utilized virtual screening methods to identify molecules in the NCI diversity set that bind SL3 RNA. The strategy of sequentially filtering the library according to molecular chemical characteristics, followed by docking using DOCK and then AutoDock, allowed us to identify compounds that bind SL3 RNA. Nine of the molecules identified bound RNA with micromolar affinity. Most of these molecules have not been shown previously to bind RNA, demonstrating that the docking methods can identify new RNA-binding ligands. Two molecules, **9** and **5**, bind with higher affinity to SL3 RNA than to double- and single-stranded RNA, and **9** shows selectivity for SL3 RNA over SL2 and SL4 RNAs. Footprinting studies have suggested that both of these molecules bind to the stem region of SL3 RNA. MD simulations predicted structures that were, in general, consistent with the experimental data. Both the MD simulations and CD experiments suggested that **9** and **5** do not alter the structure of the RNA upon binding and do not intercalate into the RNA. Because of their small size and their well-positioned points of possible modification, lead compounds **9** and **5** could form the basis for the development of high affinity small molecules that specifically recognize SL3 RNA.

Experimental Section

Materials. RNA sequences were obtained from Dharmacon Research Inc. (Lafayette, CO). RNA sequences were first deprotected and lyophilized following the procedure provided by Dharmacon. The lyophilized RNA samples were then desalted by ethanol precipitation and their purity and identity confirmed by MALDI mass spectrometry. Before any experiment, single-stranded and stem loop RNA samples were heated at 90−95 °C for 2 min and then allowed to cool slowly to room temperature. Double-stranded RNA was immediately placed on ice for 1−2 min after heating. All the compounds utilized in these investigations were obtained from the Drug Synthesis and Chemistry Branch, Development Therapeutics Program, Division of Cancer Treatment and Diagnosis, National Cancer

Institute (Bethesda, MD). The NCI diversity set is a free library from the National Cancer Institute. Compounds were identified by ESI mass spectrometry and were determined to be ≥95% pure by HPLC. The purity of **5** and **9** was confirmed using elemental analysis (CHN).

Computational Studies. Computational docking was performed on a Silicon Graphics Origin 200 with a CPU of 4 × R10000 at 180 MHz, 512 MB RAM, and an Irix 6.5.5 operating system. DOCK 5.1.1 was provided free of charge by UCSF,[37,38] and AutoDock 3.0 was obtained from the Molecular Graphics Laboratory of the Scripps Research Institute.[39] MOE from Chemical Computing Group was used to add atomic partial charges using the Gasteiger (PEOE) force field to the RNA and the ligands on a desktop PC with a Pentium4 processor, CPU 3.00 GHz with 2.00 GB of RAM running windows XP professional operating system.

For the MD simulations, the ligands, RNA, and complexes were minimized and equilibrated on a Silicon Graphics Origin 200 with a CPU of 4 × R10000 at 180 MHz, 512 MB RAM. and an Irix 6.5.5 operating system, and the 5 ns simulations were performed on a Sun Workstation with a 64-bit AMD Opteron processor, 8 GB RAM (Sun Microsystems Inc.). The AMBER8 suite of programs[48] and Amber98 force-field[49] were used for the MD simulations of the ligand−SL3 RNA complexes. Antechamber tool set was used with the general AMBER force field (GAFF)[62] to generate force field parameter files for the ligands for use with the AMBER simulation programs. The complexes were solvated in a truncated octahedral box of TIP3P water and the system neutralized by adding sodium counterions before minimization and equilibration using the program SANDER. All the systems were treated using the same procedure. Each system was initially minimized for 500 steps, and the water molecules and counterions were relaxed around the fixed solute with a 100 ps MD run, which was followed by a 5 ns MD production run. Bonds involving hydrogens were constrained by using the algorithm SHAKE.[63] A cutoff of 10 Å was used for nonbonded van der Waals interactions. The system temperature was maintained at 300 K, and Langevin dynamics were used to control the temperature using a collision frequency of 1.0 ps^{-1}. Isotropic position scaling was used to maintain a constant pressure of 1 atm with a relaxation time of 3 ps. Periodic boundary conditions were applied and the particle-mesh Ewald method was used to treat electrostatic interactions.

Fluorescence Experiments. Fluorescence experiments were performed on a FluoroMax-3 fluorimeter (Horiba Jobin Yvon). RNA (25 nM) labeled with fluorescein at the 5′ end was prepared in fluorescence binding buffer (10 mM Tris-HCl (pH 7.4) and 25 mM NaCl). The RNA sample (250 μL) was then placed in a thoroughly cleaned and dried 3 mm × 3 mm path length quartz fluorescence microcuvette (Starna Cells, Inc.) along with a 2 mm × 2 mm spin bar. The spin bar did not interfere with the light path of the spectrometer.

Three methods were used to measure dissociation constants of the RNA−small molecule complexes. In the first, fluorescein-labeled RNA was excited at 490 nm with a 3 nm band pass, and the emission fluorescence signal was monitored at 510−530 nm with an 8 nm band pass. Aliquots (1 μL) of a stock solution of the ligand were sequentially added to the RNA sample at 25 °C until the fluorescence signal was fully saturated, allowing 3−5 min for equilibration after each addition. The signal at 517 nm was used to determine the K_D's for all compounds, except for **9**, for which the signal at 525 nm was used. The fluorescence titration data were fit to a 1:1 binding model of RNA and ligand using eq 1.[51,64]

$$(F - F_0)/(F_f - F_0) = (a \times [x]_T)/(K_D + [x]_T) \quad (1)$$

F is fluorescence intensity of the sample, F_0 is the initial fluorescence intensity, F_f is the final fluorescence intensity, a is the asymptotic limit, $[x]_T$ is the total ligand concentration, and K_D is the dissociation constant. All binding measurements were performed with a greater than 10-fold excess of ligand over RNA in each binding reaction so that $[x]$ is approximately equal to $[x]_T$.

In the second method, changes in the fluorescence signal of the small molecules (10 μM **4** and 5 μM **2**) upon addition of 14mer SL3 RNA were monitored. Compound **2** was excited at 270 nm, the emission was monitored from 284 to 350 nm, and the emission at 300 nm was used for K_D determination. Compound **4** was excited at 287 nm, the emission was monitored from 450 to 490 nm, and emission at 470 nm was used for K_D determination. Equation 1 was used to fit the data and determine the K_D.

The K_D of **5** for SL4 was determined by a third method in which the RNA was labeled in the loop by substituting adenine at position 9 with 2-aminopurine. The 2-aminopurine labeled SL4 RNA was excited at 310 nm with a 4 nm band pass and the emission monitored at 350−420 nm with a 12 nm band pass. The 2-aminopurine labeled SL4 (250 nM) was then titrated with **5** following similar procedures as described above for the experiments performed with the fluorescein-labeled RNA and the data were analyzed and fit with eq 1 to determine the K_D.

ITC Experiments. In a standard experiment, aliquots of the ligand solution (10 μL, 500 μM) were added to the sample cell that contained the RNA (20 μM, 1.42 mL) at 25 °C using a 250 μL rotating syringe (300 rpm). Both the ligand and RNA were in a buffer comprised of 10 mM Tris·HCl (pH 7.4) and 25 mM NaCl. Each experiment was accompanied by a control experiment in which aliquots of the ligand were titrated into buffer alone at 25 °C. The duration of each injection was 24 s, and the spacing between two consecutive injections was 240 s. The initial delay before the first injection was 60 s. The instrument measured heat release from each injection in $\mu cal \cdot s^{-1}$. Heat release for each injection was measured by determining the area under the curve using Origin 5.0 software (MicroCal, Inc., Northampton, MA). The heat of ligand binding for each injection was determined by subtracting ligand−buffer solvation from the heat associated with corresponding ligand−RNA injection. Dissociation constants were determined from plots of heat of ligand binding as a function of ligand−RNA molar ratio. Data were fit using a sequential two-site binding model.

CD Spectroscopy. CD experiments were carried out using a JASCO J-715 spectropolarimeter. Increasing amounts of each compound were titrated into a solution of SL3 RNA (15 μM in 10 mM Tris·HCl (pH 7.4), 25 mM NaCl) at 25 °C. Control experiments were performed in which similar volumes of buffer were titrated into the RNA solution. At least three spectral scans were accumulated from 230 to 320 nm using a cell with a 0.2 cm path length.

Footprinting Studies. The reaction mixture (10 μL) was made by mixing ^{32}P-labeled RNA (1 μL, 25 nM), with corresponding ligand (1 μL) at a series of concentrations, lead acetate (1 μL, 10 mM), and buffer (7 μL, 10 mM Tris·HCl pH 7.4, 50 mM KCl). Two control experiments were performed: one was a reaction mixture comprised of RNA (1 μL, 25 nM) and 9 μL of buffer; another was a reaction mixture comprised of RNA (1 μL, 25 nM), lead acetate (1 μL, 10 mM), and buffer (8 μL). The mixture of RNA and each of the ligands were incubated at room temperature for 30 min, and then lead acetate was added to the mixture and allowed to react for 5 min at 25 °C. The reactions were quenched by addition of 10 μL of 20 mM EDTA, 8 M urea. The RNA samples were heated at 95 °C for 5 min and resolved on a 20% polyacrylamide denaturing gel (1.08% Tris base, 0.55% boric acid, and 0.06% EDTA in water, 40 W, 3 h). Gels were analyzed using a STORM 840 imager. The relative percent protection was determined by calculating the difference between the intensity of each RNA band in the presence and absence of the ligand, dividing by the intensity of the RNA band in the absence of ligand, and multiplying by 100.

UV Melting Experiments. UV melting experiments were performed in Tris·HCl (10 mM, pH 7.4) and 25 mM NaCl

buffer. Absorbance changes were monitored from 20 to 100 °C with a ramp rate of 0.5 $K \cdot min^{-1}$. The results were fit to a two-state transition model with a sigmoidal algorithm using KaleidaGraph 3.5 (Synergy Software). The two-state transition equation is:

$$a + (b - a)/(1 + (x/c)^d)$$

Where a is the maximum absorbance at 260 nm, b is the minimum absorbance at 260 nm, c is the temperature at the midpoint of absorbance, and d is the slope at the midpoint of absorbance.

Acknowledgment. Compounds that were experimentally tested for binding to RNA were provided by the National Cancer Institute. We thank Dr. David Beveridge, Dr. Surjit Dixit, Dr. Sergei Ponomarev, and Dr. Bethany Kormos for assistance with MD studies and Dr. Zhaohui Yan for assistance with docking studies. This research was supported by the University of Illinois and a Mellon New Initiative grant from Wesleyan University.

References

(1) Nierhaus, K. H.; Wilson, D. N. Protein Synthesis and Ribosome Structure: Translating the Genome; Wiley-VCH: *Weinheim, Germany*, 2004.
(2) Bloomfield, V. A.; Crothers, D. M.; Tinoco, I., *Nucleic Acids: Structures, Properties, and Functions*; University Science Books: Sausalito, CA, 2000.
(3) Thomas, J. R.; Hergenrother, P. J. Targeting RNA with Small Molecules. *Chem. Rev*. **2008**, *108*, 1171–1224.
(4) Chow, C.; Bogdan, F. A structural basis for RNA−ligand interactions. *Chem. Rev*. **1997**, *97*, 1489–1513.
(5) Sucheck, S. J.; Wong, C. H. RNA as a target for small molecules. *Curr. Opin. Chem. Biol*. **2000**, *4*, 678–686.
(6) Be′langer, F. G.; M., G.; Steinberg, S. V.; Cunningham, P. R.; Brakier-Gingras, L. Study of the functional interaction of the 900 tetraloop of 16S ribosomal RNA with helix 24 within the bacterial ribosome. *J. Mol. Biol*. **2004**, *338*, 683–693.
(7) Costa, M.; Deme, E.; Jacquier, A.; Michel, F. Multiple tertiary interactions involving domain II of group II self-splicing introns. *J. Mol. Biol*. **1997**, *267*, 520–536.
(8) Costa, M.; Michel, F. Frequent use of the same tertiary motif by self-folding RNAs. *EMBO J*. **1995**, *14*, 1276–1285.
(9) Hedenstierna, K. O. F.; Siefert, J. L.; Fox, G. E.; Murgola, E. J. Co-conservation of rRNA tetraloop sequences and helix length suggests involvement of the tetraloops in higher-order interactions. *Biochimie* **2000**, *82*, 221–227.
(10) Ikawa, Y.; Naito, D.; Aono, N.; Shiraishi, H.; Inoue, T. A conserved motif in group IC3 introns is a new class of GNRA receptor. *Nucleic Acids Res*. **1999**, *27*, 1859–1865.
(11) Klosterman, P. S.; Hendrix, D. K.; Tamura, M.; Holbrook, S. R.; Brenner, S. E. Three dimensional motifs from the SCOR, structural classification of RNA database: extruded strands, base triples, tetraloops and U-turns. *Nucleic Acids Res*. **2004**, *32*, 2342–2352.
(12) Krummel, D. A. P.; Altman, S. Verification of phylogenetic predictions in vivo and the importance of the tetraloop motif in a catalytic RNA. *Proc. Natl. Acad. Sci. U.S.A*. **1999**, *96*, 11200–11205.
(13) Varani, G. Exceptionally stable nucleic acid hairpins. *Annu. Rev. Biophys. Biomol. Struct*. **1995**, *24*, 379–404.
(14) Woese, C. R.; Gutell, R.; Gupta, R.; Noller, H. F. Detailed analysis of the higher-order structure of 16s-like ribosomal ribonucleic-acids. *Microbiol. Rev*. **1983**, *47*, 621–669.
(15) Woese, C. R.; Winker, S.; Gutell, R. R. Architecture of ribosomal RNA: constraints on the sequence of "tetra-loops". *Proc. Natl. Acad. Sci. U.S.A*. **1990**, *87*, 8467–8471.
(16) Yan, Z.; Sikri, S.; Beveridge, D. L.; Baranger, A. M. Identification of aminoacridine derivative that binds to RNA tetraloops. *J. Med. Chem*. **2007**, *50*, 4096–4104.
(17) Clever, J. L.; Parslow, T. G. Mutant human immunodeficiency virus type 1 genomes with defects in RNA dimerization or encapsidation. *J. Virol*. **1997**, *71*, 3407–3414.
(18) De Guzman, R. N.; Wu, Z. R.; Stalling, C. C.; Pappalardo, L.; Borer, P. N.; Summers, M. F. Structure of the HIV-1 nucleocapsid protein bound to the SL3 psi-RNA recognition element. *Science* **1998**, *249*, 384–388.
(19) Clever, J. L.; Eckstein, D. A.; Parslow, T. G. Genetic dissociation of the encapsidation and reverse transcription functions in the 5′ R region of human immunodeficiency virus type 1. *J. Virol*. **1999**, *73*, 101–109.
(20) Clever, J.; Sassetti, C.; Parslow, T. G. RNA secondary structure and binding sites for gag gene products in the 5′ packaging signal of human immunodeficiency virus type 1. *J. Virol*. **1995**, *69*, 2101–2109.
(21) Damgaard, C. K.; Dyhr-Mikkelsen, H.; Kjems, J. Mapping the RNA binding sites for human immunodeficiency virus type-1 Gag and NC proteins within the complete HIV-1 and -2 untranslated leader regions. *Nucleic Acids Res*. **1998**, *26*, 3667–3676.
(22) Hayashi, T.; Shioda, T.; Iwakura, Y.; Shibuta, H. RNA packaging signal of human immunodeficiency virus type 1. *Virology* **1992**, *188*, 590–599.
(23) Lucia, P.; Deborah, J. K.; István, P.; Philip, N. B. Three-dimensional folding of an RNA hairpin required for packaging HIV-1. *J. Mol. Biol*. **1998**, *282*, 801–818.
(24) McBride, M. S.; Panganiban, A. T. The human immunodeficiency virus type 1 encapsidation site is a multipartite RNA element composed of functional hairpin structures. *J. Virol*. **1996**, *70*, 2963–2973.
(25) McBride, M. S.; Panganiban, A. T. Position dependence of functional hairpins important for human immunodeficiency virus type 1 RNA encapsidation in vivo. *J. Virol*. **1997**, *71*, 2050–2058.
(26) McBride, M. S.; Schwartz, M. D.; Panganiban, A. T. Efficient encapsidation of human immunodeficiency virus type 1 vectors and further characterization of cis elements required for encapsidation. *J. Virol*. **1997**, *71*, 4544–4554.
(27) Michael, F. S.; Andrew, C. P.; Bruce, S. H.; Philip, N. B. Affinities of packaging domain loops in HIV-1 RNA for the nucleocapsid protein. *Biochemistry* **2002**, *41*, 5276–5282.
(28) Hayashi, T.; Ueno, Y.; Okamoto, T. Elucidation of a conserved RNA stem−loop structure in the packaging signal of human immunodeficiency virus type 1. *FEBS Lett*. **1993**, *327*, 213–218.
(29) Turner, K. B.; Hagan, N. A.; Fabris, D. Inhibitory effects of archetypical nucleic acid ligands on the interactions of HIV-1 nucleocapsid protein with elements of psi-RNA. *Nucleic Acids Res*. **2006**, *34*, 1305–1316.
(30) McPike, M. P.; Goodisman, J.; Dabrowiak, J. C. Footprinting and Cirular Dichroism Studies on Paromomycin Binding to the Packaging Region of Human Immunodeficiency Virus Type-1. *Bioorg. Med. Chem*. **2002**, *10*, 3663–3672.
(31) McPike, M. P.; Goodisman, J.; Dabrowiak, J. C. Specificity of neomycin analogues bound to the packaging region of human immunodeficiency virus type 1 RNA. *Bioorg. Med. Chem*. **2004**, *12*, 1835–1843.
(32) McPike, M. P.; Sullivan, J. M.; Goodisman, J.; Dabrowiak, J. C. Footprinting, circular dichroism and UV melting studies on neomycin B binding to the packaging region of human immunodeficiency virus type-1 RNA. *Nucleic Acids Res*. **2002**, *30*, 2825–2831.
(33) Yan, Z.; Baranger, A. M. Binding of an Aminoacridine Derivative to a GAAA RNA Tetraloop. *Bioorg. Med. Chem. Lett*. **2004**, *14*, 5889–5893.
(34) Pustowka, A.; Dietz, J.; Ferner, J.; Baumann, M.; Landersz, M.; Konigs, C.; Schwalbe, H.; Dietrich, U. Identification of Peptide Ligands for Target RNA Structures Derived from the HIV-1 Packaging Signal Y by Screening Phage-Displayed Peptide Libraries. *ChemBioChem* **2003**, *4*, 1093–1097.
(35) Dietz, J.; Koch, J.; Kaur, A.; Raja, C.; Stein, S.; Grez, M.; Pustowka, A.; Mensch, S.; Ferner, J.; Moller, L.; Bannert, N.; Tampé, R.; Divita, G.; Mély, Y.; Schwalbe, H.; Dietrich, U. Inhibition of HIV-1 by a peptide ligand of the genomic RNA packaging signal psi. *ChemMedChem* **2008**, *3*, 749–755.
(36) Ewing, T. J. A.; Makino, S.; Skillman, A. G.; Kuntz, I. D. DOCK 4.0: search strategies for automated molecular docking of flexible molecule databases. *J. Comput-Aided Mol. Des* **2001**, *15*, 411–428.
(37) Kuntz, I. D. Structure-based strategies for drug design and discovery. *Science* **1992**, *257*, 1078–1082.
(38) Kuntz, I. D.; Blaney, J. M.; Oatley, S. J.; Langridge, R.; Ferrin, T. E. A geometric approach to macromolecule−ligand interactions. *J. Mol. Biol*. **1982**, *161*, 269–288.
(39) Morris, G. M.; Goodsell, D. S.; Halliday, R. S.; Huey, R.; Hart, W. E.; Belew, R. K.; Olson, A. J. Automated docking using a Lamarckian genetic algorithm and an empirical binding free energy function. *J. Comput. Chem*. **1998**, *19*, 1639–1662.
(40) Barbault, F.; Zhang, L.; Zhang, L.; Fan, B. T. Parametrization of a specific free energy function for automated docking against RNA targets using neural networks. *Chemom. Intell. Lab. Syst* **2006**, *82*, 269–275.
(41) Chen, Q.; Kuntz, I. D.; Shafer, R. H., Structure-Based Design of Nucleic Acid Binding Drugs. In *Structure, Motion, Interaction and*

Expression of Biological Macromolecules; Adenine Press: New York, 1997; pp 227−231.
(42) Detering, C.; Varani, G. Validation of automated docking programs for docking and database screening against RNA drug targets. *J. Med. Chem.* **2004**, *47*, 4188–4201.
(43) Moitessier, N.; Westhof, E.; Hanessian, S. Docking of aminoglycosides to hydrated and flexible RNA. *J. Med. Chem.* **2006**, *49*, 1023–1033.
(44) Zhang, X.; Wang, X.; Liu, C. Molecular docking and 3D-QSAR study of pyranmycin derivatives against 16S rRNA A site. *J. Mol. Struct.: THEOCHEM* **2005**, *730*, 85–94.
(45) Haddad, J.; Kotra, L. P.; Liano-Sotelo, B.; Kim, C.; Azucena, E. F.; Liu, M.; Vakulenko, S. B.; Chow, C. S.; Mobashery, S. Design of Novel Antibiotics that Bind to the Ribosomal Acyltransfer Site. *J. Am. Chem. Soc.* **2002**, *124*, 3229–3237.
(46) Evans, D. A.; Neidle, S. Virtual screening of DNA minor groove binders. *J. Med. Chem.* **2006**, *49*, 4232–4238.
(47) Kuntz, I. D.Ewing, T. J. A. *DOCK Version 4.0 User Manual*; University of California: San Francisco, **1998**; pp 20−21
(48) Case, D. A.; Darden, T. A.; Cheatham, T. E.; Simmerling, C. L.; Wang, J.; Duke, R. E.; Luo, R.; Merz, K. M.; Wang, B.; Pearlman, D. A.; Crowley, M.; Brozell, S.; Tsui, V.; Gohlke, H.; Mongan, J.; Hornak, V.; Cui, G.; Beroza, P.; Schafmeister, C.; Caldwell, J. W.; Ross, W. S.; Kollman, P. A. *AMBER 8*; University of California: San Franscisco, 2004.
(49) Cheatham, T. E., III; Cieplak, P.; Kollman, P. A modified version of the Cornell et al. force field with improved sugar pucker phases and helical repeats. *J. Biomol. Struct. Dyn.* **1999**, *16*, 845–862.
(50) Llano-Sotelo, B.; Chow, C. S. RNA−aminoglycoside antibiotic interactions: fluorescence detection of binding and conformational change. *Bioorg. Med. Chem. Lett.* **1999**, *8*, 213–216.
(51) Thomas, J. R.; Liu, X.; Hergenrother, P. J. Size-specific ligands for RNA hairpin loops. *J. Am. Chem. Soc.* **2005**, *127*, 12434–12435.
(52) Llano-Sotelo, B.; Azucena, E.; Kotra, L.; Mobashery, S.; Chow, C. Aminoglycosides modified by resistance enzymes display diminished binding to the bacterial ribosomal aminoacyl-tRNA site. *Chem. Biol.* **2002**, *9*, 455–463.
(53) Li, V.-S.; Tang, M.-s.; Kohn, H. The Effect of C(5) Cytosine Methylation at CpG Sequences on Mitomycin−DNA Bonding Profiles. *Bioorg. Med. Chem.* **2001**, *9*, 863–873.
(54) Tomasz, M.; Chawla, A. K.; Lipman, R. Mechanism of Monofunctional and Bifunctional Alkylation of DNA by Mitomycin C. *Biochemistry* **1988**, *27*, 3182–3187.
(55) Li, V.-S.; Choi, D.; Tang, M.-S.; Kohn, H. Concerning in Vitro Mitomycin−DNA Alkylation. *J. Am. Chem. Soc.* **1996**, *118*, 3765–3766.
(56) Erikson, M.; Norden, B. Linear and circular dichroism of drug-nucleic acid complexes. *Methods Enzymol.* **2001**, *340*, 68–98.
(57) Ratmeyer, L.; Zapp, M. L.; Green, M. R.; Vinayak, R.; Kumar, A.; Boykin, D. W.; Wilson, W. D. Inhibition of HIV-1 Rev−RRE interaction by diphenylfuran derivatives. *Biochemistry* **1996**, *35*, 13689–13696.
(58) McPike, M. P.; Sullivan, J. M.; Goodisman, J.; Dabrowiak, J. C. Footprinting, circular dichroism and UV melting studies on neomycin B binding to the packaging region of human immunodeficiency virus type-1 RNA. *Nucleic Acids Res.* **2002**, *30*, 2825–2831.
(59) Proctor, D. J.; Schaak, J. E.; Bevilacqua, J. M.; Falzone, C. J.; Bevilacqua, P. C. Isolation and characterization of a family of stable RNA tetraloops with motif YNMG that participate in tertiary interactions. *Biochemistry* **2002**, *41*, 12062–12075.
(60) Litovchik, A.; Evdokimov, A. G.; Lapidot, A. Aminoglycoside−arginine conjugates that bind TAR RNA: synthesis, characterization, and antiviral activity. *Biochemistry* **2000**, *39*, 2838–2852.
(61) Brunel, C.; Romby, P. Probing RNA structure and RNA−ligand complexes with chemical probes. *Methods Enzymol.* **2000**, *318*, 3–21.
(62) Wang, J.; Wolf, R. M.; Caldwell, J. W.; Kollman, P. A.; Case, D. A. Development and testing of a general amber force field. *J. Comput. Chem.* **2004**, *25*, 1157–1173.
(63) Yrckaert, J. P.; C., G.; Berendsen, H. J. C. Numerical-integration of cartesian equations of motions of a system with constraints—molecular dynamics of *n*-alkanes. *J. Comput. Phys.* **1977**, *23*, 327–341.
(64) Liu, X.; Thomas, J. R.; Hergenrother, P. J. Deoxystreptamine dimers bind to RNA hairpin loops. *J. Am. Chem. Soc.* **2004**, *126*, 9196–9197.